Available online at www.sciencedirect.com
SCIENCE DIRECT®
Journal of Chromatography A, 1032 (2004) 149–158
JOURNAL OF CHROMATOGRAPHY A
www.elsevier.com/locate/chroma

Capillary electrophoresis of inorganic anions in hydro-organic media Influence of ion-pairing and solvation phenomena

Stéphanie Descroix, Anne Varenne*, Carlo Adamo, Pierre Gareil

Ecole Nationale Supérieure de Chimie de Paris, Laboratoire d'Electrochimie et Chimie Analytique, UMR CNRS 7575, 11 Rue Pierre et Marie Curie, F-75231 Paris Cedex 05, France

Abstract

The capillary electrophoresis separation of four inorganic anions (NO_3^-, I^-, Br^- and SCN^-) was investigated over the whole range of methanol–water mixture composition. As the separation selectivity was strongly dependent on the solvent composition, the influence of ion-pairing and solvation phenomena was examined in depth in an attempt to explain this modification. First, a series of experiments was performed in methanolic background electrolytes, with counter-ions of different size. Ion-pair formation involving electrolyte ions was assessed to allow for a correction for free electrolyte ion concentration. Ion-pair formation constants between each inorganic anion and electrolyte counter-ion were next determined from the variations of the anion mobility as a function of the free counter-ion concentration. In view of the low values obtained, ion-pair formation alone failed to explain the selectivity variations. Solvation phenomena were then investigated with the help of a theoretical quantum model, the density functional theory (DFT), coupled with a polarizable continuum model to mime non-specific solvent effects. Whereas this model proved successful at predicting the mobility order at infinite dilution in water, it failed to predict the correct order in methanol.

Keywords: Background electrolyte composition; Ion pairing; Solvation; Mathematical modelling; Inorganic anions

1. Introduction

Over the last decade, non-aqueous capillary electrophoresis (NACE) has undergone a rapid development for various classes of compounds including pharmaceuticals [1–4], enantiomers [5–8], surfactants [9–11], peptides [12,13], oligomers [14–16], as well as small organic and inorganic anions [17–19]. In effect, organic solvents and their mixtures provide an almost endless range of new physico-chemical properties allowing to manipulate analyte solubility, separation selectivity, electroosmotic transport and to extend detection consistency. Considering the separation selectivity, the phenomena involved can be shifts in acido–basic [20–23], or complexation equilibria [24], hydrogen bonding, interaction types which do not occur, if hardly in aqueous media, such as ion-pairing [25–27], charge transfer [28,29], heteroconjugation [17,21], modification of the dielectric friction [30,31], or of solvation shell [18,32]. While the role presumably played by these phenomena has already been reported for a deal of NACE separations, quantitative description of their effects and rationalization of their use have been the topic of a much more restrained number of papers [20,21,26,27,33,34], and one still lacks most of the analytical and physicochemical data that would be necessary for proper optimization of NACE separations. In the case of the inorganic anions, whose conjugated acids remain strong in most of the usual solvents, the solvent effects amenable to selectively impact separation may stem from ion-pairing or modification of the electrophoretic friction coefficient. Ion-pair formation can be classically demonstrated by confronting the experimental variations of analyte electrophoretic mobility versus counter-ion concentration with Debye–Hückel–Onsager [35–37], or Falkenhagen et al. [38] and Pitts [39] models. More quantitatively, ion-pair formation constants can further be calculated using an actual ion-pair model [25,40]. The modification of the electrophoretic friction coefficient, to which the electrophoretic mobility is inversely proportional, may be interpreted as the occurrence of dielectric friction and/or solvation effects. Solvation effects, which are governed at the microscopic level by ion–solvent and solvent–solvent interactions have been much more difficult to characterize on a quantitative basis till recently. These interactions can now be described

* Correspondiing author. Tel.: +33-1-55426372; fax: +33-1-44276750.
E-mail address: anne-varenne@enscp.jussieu.fr (A. Varenne).

0021-9673/$ – see front matter © 2004 Elsevier B.V. All rights reserved.
doi:10.1016/j.chroma.2003.11.070

rather accurately by theoretical models which have been classified into two groups according to the approach. The first one contains classical simulations based on molecular mechanics, molecular dynamics and classical Monte Carlo approaches, while quantum chemistry approaches are incorporated in the second group [41]. This latter approach is more suitable for describing the subtle electronic effects ruling solute–solvent interactions. While the results thus obtained appear reasonable for non-polar solvents, they are more questionable for solvents (e.g. water) where local organization (due to the hydrogen bond network) cannot be neglected. Therefore, solvation shells beyond the first one have to be included in any coherent model. Unfortunately, this extension might be troublesome for computational approaches rooted in quantum mechanics, where the computer time rapidly scales with the size of the systems under investigation. One possible way out is provided by the so-called continuum models, in which the bulk solvent is a continuum polarizable medium representing, on an average, all the possible conformations accessible to the solvent molecules [42]. This latter model has given accurate results for molecular properties and thermodynamic parameters in polar, hydrogen-bonded liquids [43–46].

A combined experimental and theoretical study is presented here for a better understanding of the selectivity alterations observed for some model inorganic anions (chloride, bromide, nitrate, thiocyanate) on varying the solvent composition (water–methanol mixtures) of the background electrolyte. For this aim, ion-pairing contribution was first evaluated in purely methanolic media by studying the variation of the electrophoretic mobilities of these four anions as a function of the concentration of the counter-ion present in the electrolyte. This study was performed with two counter-ions of different size. The occurrence of association between the electrolyte ions was checked beforehand in order to possibly correct for the free counter-ion concentration. The assessment of solvation contribution was next conducted on the basis of theoretical microscopic quantum chemistry by calculating the solvated radii for each anion, both in water and methanol. Density functional theory (DFT) and conductor-like polarizable continuum model (CPCM) computations have been carried out to relate the experimental outcomes to the microscopic organization of the solvent around the anionic solutes.

2. Materials and methods

2.1. Chemicals

Perchloric acid, ethanolamine, ammediol, benzyl alcohol, sodium bromide, sodium nitrate, sodium thiocyanate, and potassium nitrate were purchased from Sigma–Aldrich (Saint-Quentin Fallavier, France) and sodium iodide was from Prolabo (Paris, France). HPLC-grade methanol (MeOH) was also supplied by Prolabo. Water used throughout was produced by an Alpha Q laboratory water-purification system (Millipore, Molsheim, France).

2.2. Capillary electrophoresis

CE experiments were carried out with an HP ^{3D}CE apparatus (Agilent, Waldbronn, Germany) equipped with a diode-array detector, an autosampler and a power supply able to deliver up to 30 kV. Data were handled by an HP Chemstation software. Bare fused silica capillaries, 40 cm (31.5 cm from inlet to detector) × 50 μm i.d. and 360 μm o.d., were from Beckman (Gagny, France). Samples were introduced in the hydrodynamic mode (30 mbar/3 s). Separations were performed under a negative voltage of 15 kV and the temperature in the capillary cartridge was set at 25 °C. Absorbance detection was carried out at 200 nm. The acquisition rate of the detector signal was 10 points s^{-1}.

The background electrolytes (BGEs) consisted of ethanolamine and perchloric acid or ammediol and perchloric acid of various concentrations but of constant (2:1) molar ratio, in MeOH–water solvent mixtures. All electrolytes were filtered through 0.2 μm filter units before use. The samples of inorganic anions were prepared in water at concentrations between 40 and 80 ppm. Benzyl alcohol (1% (v/v), in water) was used as a neutral marker for the determination of the electroosmotic mobility. New capillaries were conditioned by successive flushes with 1 and 0.1 M NaOH and then with water, for 10, 5 and 10 min, respectively, under a pressure of 900 mbar. Prior to each sample injection, the capillary was rinsed with the separation electrolyte for 5 min. Capillaries were rinsed with water and dried by air when not in use. Each sample was injected several times to check repeatability of the data.

2.3. Conductivity measurements

The conductivity of each BGE was directly measured at 25.0 ± 0.5 °C using a Radiometer CDM210 conductimeter (Villeurbanne, France). The cell constant was determined by calibration with various concentrations (10^{-1} to 10^{-3} M) of potassium chloride.

2.4. Computational procedures

All DFT calculations were carried out with our modified version of the Gaussian'98 code [47], using a hybrid Kohn–Sham/Hartree–Fock (KS/HF) model referred to B1LYP [48]. This approach was obtained casting the Becke exchange [49] and the Lee et al. correlation functionals [50] in an hybrid scheme HF/DFT, where the HF exchange ratio (1/4) was fixed a priori. The geometry of all the considered cluster systems was fully optimized using the 6–311 + G(d, p) basis set [51]. All the interaction energies were corrected for zero point energies (ZPE) and basis set superposition error contributions [52].

Solvent effects were evaluated using the so-called polarizable continuum model (PCM) [42]. In particular, optimized structures and solvation energies were computed by a cavity model, namely the united atoms topological model (UATM) [53], coupled to the CPCM [54]. This approach has provided results very close to those obtained by the original dielectric model for high dielectric constant solvents, but it has been significantly more effective in geometry optimizations and less prone to numerical errors arising from the small part of the solute electron cloud lying outside the cavity (escaped charge effects). Cluster volumes were then evaluated by a Monte Carlo integration, either in gas phase or in solution, as the region of space occupied by the 99% of the electron density [51]. Solvated radii were finally calculated as the radii of the spheres having the same volume.

3. Results and discussion

3.1. Effect of solvent composition on the actual mobility of the inorganic anions

The electrophoretic behaviour of bromide, iodide, nitrate and thiocyanate was first studied with a fixed 12 mM ethanolamine–6 mM perchloric acid background electrolyte over the whole range of methanol–water compositions (10–100% methanol). The electroosmotic mobility inside the bare silica capillary was observed to decrease steadily in the range of 0–70% methanol and then to stabilize for methanol contents over 70%. This behaviour was similar to what has been already reported by others [13,18,55] and was explained by both a decrease in the dielectric constant to viscosity ratio (in the 0–60% range) and in the zeta potential of silica (absolute value, mainly in the 30–100% range) on increasing methanol content [55]. For methanol contents higher than 10%, the electroosmotic mobility becomes much lower than the electrophoretic mobility of all four inorganic anions (in absolute value), so that the anions migrate fast towards the anode compartment counter-electroosmotically. The electrophoretic mobility of the four anions was thus determined as a function of the methanol content in the 10–100% range. As shown in Fig. 1A, these mobilities go through a minimum value for methanol contents of ca. 50–60%. Although this overall tendency mostly reflects the variation of the reciprocal viscosity of methanol–water mixtures [55], the product of the mobility by the viscosity (Walden's product) does not remain constant over the whole range of methanol content (Fig. 1B), which demonstrates that other parameters than viscosity should influence the mobility of the four anions. In agreement with previous observations by other groups [56,57], several changes in migration orders were also noticed over the range of methanol content studied (Fig. 1A), which cannot be either attributed to a viscosity effect. The pH of the background electrolyte, which corresponds to the pK_a of ethanolamine in the solvent medium, should not much vary over the range

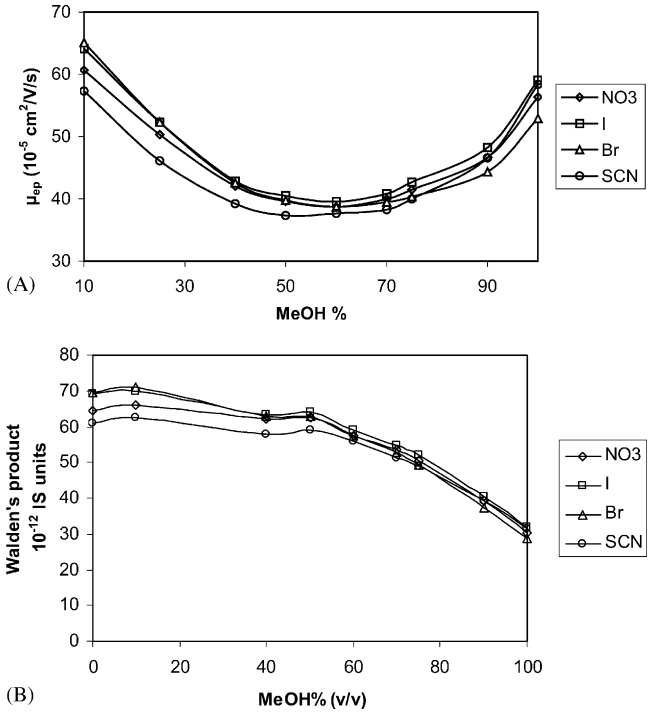

Fig. 1. Effect of solvent composition on: (A) the electrophoretic mobilities of the four model inorganic anions and (B) the product of the electrophoretic mobility by the electrolyte viscosity. Electrolyte: 12 mM ethanolamine, 6 mM perchloric acid in methanol–water mixtures of various compositions. Temperature: 25 °C.

of methanol composition, as ethanolamine is a B/BH^+ type buffer. Anyway, this slight variation cannot affect the measured mobilities of the four anions studied, since they should remain extremely weak bases in these solvent media. The observed deviations from the constancy of Walden's products may rather be attributed to ion-pairing or friction coefficient modification due to dielectric friction and/or solvation phenomena. The present discussion will focus solely on the influence of ion-pairing and solvation. As an application of this, Fig. 2 shows the separations of the four anions (A) in pure methanol and (B) in a methanol–water (75:25 (v/v)) mixture. While these anions are fully resolved in both media, it is worth noting that the migration orders are different in conditions (A) $I^- < SCN^- < NO_3^- < Br^-$ and (B) $I^- < NO_3^- < Br^- < SCN^-$, whereas the migration order in water is $Br^- < I^- < NO_3^- < SCN^-$. Furthermore, due to the higher anion mobilities in pure methanol, shorter migration times can be obtained in this medium without using any electroosmotic flow reversing agent.

3.2. Evaluation of the ion pairing between the BGE ions

In order to elucidate the phenomena implied in the selectivity modification, the ion-pairing phenomenon in the BGE itself was first studied. The aim of this investigation was also to determine the actual concentration of the

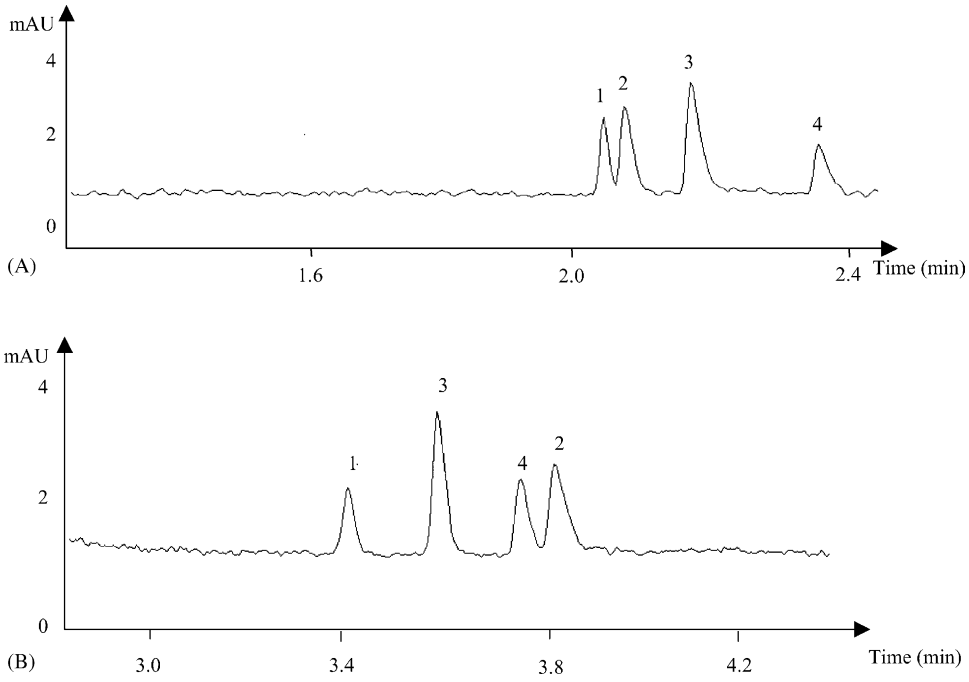

Fig. 2. Separation of model inorganic anions in: (A) pure methanol and (B) a water–methanol (25:75 (v/v)) mixture. Fused silica capillary, 40 cm (detection, 31.5 cm) × 50 μm i.d. Electrolyte: 12 mM ethanolamine, 6 mM perchloric acid. Applied voltage: −20 kV. Temperature: 25 °C. Hydrodynamic injection: 30 mbar, 3 s. Absorbance detection at 200 nm. Peak identification and analyte concentrations: (1) I^-, 60 ppm; (2) SCN^-, 80 ppm; (3) $NO_3{}^-$, 40 ppm; (4) Br^-, 70 ppm.

free ions of the BGE amenable to interact with the analytes. This study was conducted in a purely methanolic medium as this medium was the most favourable to yield ion-pairing, due to its lowest dielectric constant, as compared with water–methanol media. Two different buffers, ethanolamine–perchloric acid and ammediol–perchloric acid of like molar ratio (2:1), were tested in pure methanol, in order to investigate the effect of the counter-ion size. The perchloric acid concentration was varied over the range of 2–12.5 mM. Ion-pair formation between electrolyte ions was expected to lower the electrolyte equivalent conductivity. The specific conductivity σ of the electrolytes, directly obtained by conductivity measurements, were converted into equivalent conductivity Λ, according to the relationship:

$$\Lambda = \frac{\sigma}{zc} \tag{1}$$

where c and z stand for the introduced perchloric acid concentration and number of elementary charges, respectively. According to the simple Debye–Hückel–Onsager (DHO) model, the equivalent conductivity Λ for a strong 1:1 electrolyte decreases linearly with the square-root of its concentration c [35–37]:

$$\Lambda = \Lambda^\infty - (A\,\Lambda^\infty + B)c^{1/2} \tag{2}$$

with

$$A = \frac{0.82 \times 10^6}{(\varepsilon T)^{3/2}} \tag{2'}$$

and

$$B = \frac{82}{\eta(\varepsilon T)^{1/2}} \tag{2''}$$

where Λ^∞ is the electrolyte equivalent conductivity at infinite dilution, T the absolute temperature, ε the relative dielectric constant and η the viscosity of the solution. For both ethanolamine- and ammediol-based BGEs, the variation of the experimental equivalent conductivity with the square root of the introduced perchloric acid concentration remains almost linear in the concentration range investigated (Fig. 3, solid lines). For both electrolytes, the equivalent conductivities at infinite dilution were obtained as the Y-intercept of the linear regression: $\Lambda^\infty = 134 \pm 2\,\mathrm{S\,cm^2}$ per equivalent for ethanolamine-based electrolyte and $\Lambda^\infty = 127 \pm 2\,\mathrm{S\,cm^2}$ per equivalent for ammediol-based electrolyte. Using these values and the ε and η values for methanol at 25 °C (32.7 and 0.54×10^{-3} Pa s, respectively), the A and B coefficients of the DHO model were next calculated, which in turn allowed us to represent the theoretical variation of the equivalent electrolyte conductivities, according to this model (Fig. 3, broken lines). As the slopes of the experimental and theoretical straight lines were very similar, it can be concluded that ion-pairing does not occur (or occur to a very minor extent) in the neat methanolic electrolyte investigated. This result all the best applied to water–methanol mixtures which present higher dielectric constants, and eventually the free ion concentration in the electrolytes was, therefore, equal to the analytical salt concentration, whatever the methanol content was.

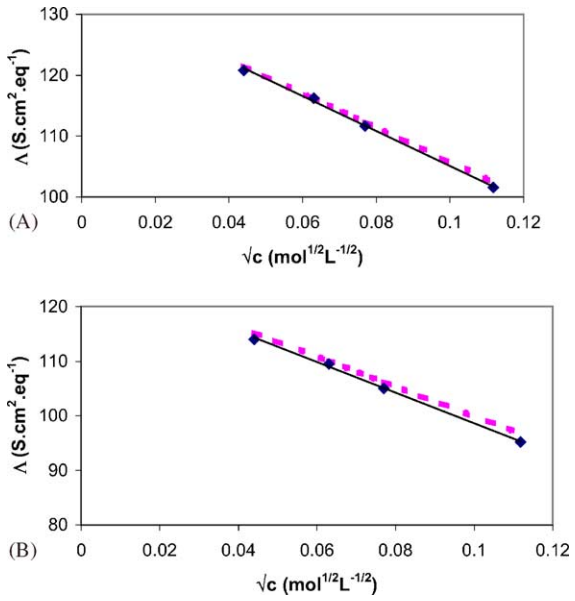

Fig. 3. Influence of the perchloric acid concentration introduced in the electrolyte on its equivalent conductivity Λ at 25 °C. (A) ethanolamine–perchloric acid buffer (molar ratio, 2:1) in pure methanol. (B) ammediol–perchloric acid buffer (molar ratio, 2:1) in pure methanol. Solid lines: least-squares linear regression of the experimental points: (A) $y = -286.62x + 133.77$, $R^2 = 0.9979$, $n = 4$, (B): $y = -280.52x + 126.67$, $R^2 = 0.9981$, $n = 4$. Broken lines: theoretical slope of the plot, according to the simple Debye–Hückel–Onsager model. See text for additional details.

3.3. Evaluation of the ion-pairing between the analytes and the BGE counter-ion

In order to evaluate the occurrence of ion-pairing between the analytes and the BGE counter-ion, the mobilities of the inorganic anions were measured in pure methanolic media using the same two buffers as those for the study of ion-pairing within electrolyte ions and the perchloric acid concentration was varied between 2 and 12.5 mM. The results were first analysed according to the models by Falkenhagen et al. [38] and Pitts [39] (FP model), to discriminate between ionic strength and ion-pairing effects. For an uni-univalent electrolyte, the actual mobility μ_i^0 of ion i was expressed as a function of ionic strength I according to:

$$\mu_i^0 = \mu_i^\infty - \left[\left(\frac{8.20 \times 10^5 \mu_i^\infty}{(\varepsilon T)^{3/2}}\right) + \frac{42.75}{\eta(\varepsilon T)^{1/2}}\right] \times \left[\frac{\sqrt{I}}{(1 + 50.29a(\varepsilon T)^{-1/2}\sqrt{I})}\right] \quad (3)$$

where μ_i^∞ is the absolute mobility and a the distance of closest approach between ion i and its counter-ion. For unit consistency, η should be taken in 10^{-1} Pa s, a in Å, I in mol l^{-1} and μ_i^∞ in 10^{-5} cm^2 V^{-1} s^{-1}. The terms $8.20 \times 10^5 \mu_i^\infty/(\varepsilon T)^{3/2}$ and $42.75/\eta(\varepsilon T)^{1/2}$ describe the relaxation and electrophoretic effects, respectively. The denominator of the last term between the brackets in Eq. (3) is unit if the ions are considered as point charges ($a = 0$), and in this case mobility is expected to decrease linearly with $\sqrt{I}$, with the so-called Onsager limiting slope. Parameter a can be estimated as the sum of the Stokes radii of the analyte and counter-ion [58], the Stokes radius $R_{St,i}$ of ion i being defined by:

$$R_{St,i} = \frac{z_i e}{6\pi\mu_i^\infty \eta} \quad (4)$$

where z_i is the charge number of ion i and e the elementary charge.

The μ_i^∞ values of I^-, SCN^-, NO_3^- and Br^- were first estimated by extrapolating at zero ionic strength the linear regression of the actual mobility of each anion versus the square-root of the BGE ionic strength. Table 1 reports the so-obtained μ_i^∞ values for both the ethanolamine- and ammediol-based electrolytes along with literature values [59]. The high calculated linear regression coefficients testify for the validity of the approach. For each anion, the μ_i^∞ values for both electrolytes and from literature show no significant difference. Table 1 also shows that the slopes of these regression straight lines did not differ significantly from the Onsager limiting slopes calculated for methanol from Eq. (3) using the extrapolated μ_i^∞ values. Nevertheless, to apply FP model and thus gain a deeper evaluation of the analyte status, the distance of closest approach was calculated for the four model anions, in both ethanolamine- and ammediol-based BGEs (Table 2). Fig. 4 shows that the actual mobilities experimentally determined as a function of the ionic strength did not match the variation calculated according to the FP model (Eq. (3)), using the preceding μ_i^∞ and a values. The fact that the departure of the experimental points from the theoretical curve is increasing with ionic strength suggests that ion-pairing between the analytes and electrolyte counter-ions may occur. In order to confirm this hypothesis, the experimental mobility data were then reprocessed according to a classical ion-pair formation model, assuming the formation of a neutral ion-pair of 1:1 stoichiometry between analyte ion i and electrolyte counter-ion C. The effective mobility of analyte i, μ_i^{eff}, can then be expressed as a function of the ion-pair formation constant K_{IP} and the free counter-ion concentration $[C]$ [25,40]:

$$\frac{\mu_i^0}{\mu_i^{eff}} - 1 = K_{IP}[C] \quad (5)$$

The plot of the left-hand term of Eq. (5) calculated from experimental values of μ_i^{eff} in terms of the free counter-ion concentration should lead to a straight line, the slope of which yields the ion-pair formation constant K_{IP}. Table 3 gives the K_{IP} values so calculated for each anion and both counter-ions, with the corresponding linear regression coefficients. The low precision of the K_{IP} determinations could be due to the fact that the levels of the free counter-ion concentration studied (2–12.5 mM) were rather low and thus ion pairs were formed in low proportions. These results show that the experimental mobility data can be reasonably well interpreted by the ion-pair formation model. The K_{IP}

Table 1
Absolute mobilities (*Y*-intercepts) and slopes obtained by linear regression of the actual mobility of the four model anions vs. the square-root of the BGE ionic strength

Analyte anions	Ethanolamine-based BGE			Ammediol-based electrolyte			μ^∞ (literature values [59]) (10^{-5} cm^2 V^{-1} s^{-1})	Onsager limiting slope (10^{-5} cm^2 V^{-1} s^{-1} mol$^{-1/2}$ l$^{1/2}$)
	μ^∞ (10^{-5} cm^2 V^{-1} s^{-1})	Experimental slope (10^{-5} cm^2 V^{-1} s^{-1} mol$^{-1/2}$ l$^{1/2}$)	Regression coefficient, R^2 ($n = 4$)	μ^∞ (10^{-5} cm^2 V^{-1} s^{-1})	Experimental slope (10^{-5} cm^2 V^{-1} s^{-1} mol$^{-1/2}$ l$^{1/2}$)	Regression coefficient, R^2 ($n = 4$)		
I^-	65.4 ± 1.9	−122.8 ± 18.0	0.99	65.4 ± 4.3	−132.8 ± 40.7	0.98	64.9	−136
SCN^-	64.8 ± 0.9	−121.0 ± 9.1	0.99	64.5 ± 3.4	−132.7 ± 32.4	0.98	64.2	−135
NO_3^-	62.9 ± 1.1	−135.8 ± 12.0	0.99	63.1 ± 2.9	−143.0 ± 27.4	0.99	63.1	−134
Br^-	60.1 ± 2.4	−130.0 ± 22.7	0.99	59.2 ± 1.8	−124.9 ± 17.3	0.99	60.1	−131

Electrolyte: ethanolamine– or ammediol–perchloric acid (molar ratio 2:1) in pure methanol, range of perchloric acid concentration studied: 2–12.5 mM. Temperature: 25 °C.

Table 2
Distances of closest approach between analyte anions and electrolyte counter-ions (parameter *a*) calculated as the sum of the Stokes radii of the analyte and counter-ion

Analyte anions	*a* (nm)	
	Ethanolamine counter-ion	Ammediol counter-ion
I^-	0.479	0.507
SCN^-	0.482	0.510
NO_3^-	0.484	0.516
Br^-	0.504	0.532

The Stokes radii of the analyte anions were calculated from Eq. (4). For the counter-ions the Stokes radii were calculated from equivalent conductivities at infinite dilution [27], the equivalent conductivity of perchloride being taken from [59].

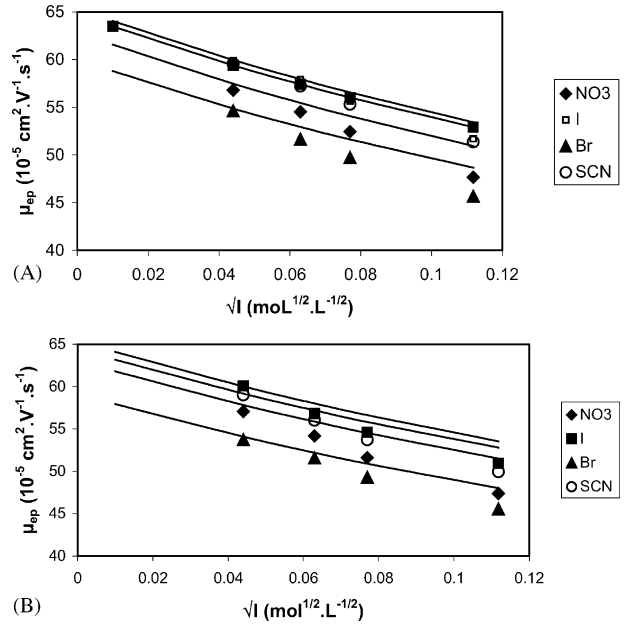

Fig. 4. Effect of electrolyte ionic strength on model anion actual mobilities. Electrolyte: (A) ethanolamine– or (B) ammediol–perchloric acid (molar ratio, 2:1) in pure methanol. Other conditions as in Fig. 2. Symbols, experimental points; solid lines, theoretical variations, according to Falkenhagen and Pitts model.

Table 3
Ion-pair formation constants (K_{IP}) between the inorganic anions and the electrolyte counter-ion in methanol, determined as the slopes of the regression straight lines, from Eq. (5)

Analyte anion	Ethanolamine counter-ion		Ammediol counter-ion	
	K_{IP} (L mol^{-1})	R^2 ($n = 4$)	K_{IP} (L mol^{-1})	R^2 ($n = 4$)
NO_3^-	5.9 ± 2.1	0.98	7.3 ± 4.5	0.96
Br^-	5.7 ± 3.5	0.96	5.2 ± 4.8	0.97
I^-	3.5 ± 2.6	0.94	4.8 ± 3.1	0.87
SCN^-	3.3 ± 0.8	0.99	4.9 ± 3.1	0.91

The least-squares regression coefficients (R^2) are also given.

Table 4
Solvated radii of the model inorganic anions in water and methanol estimated from the Stokes hydrodynamic radii (Eq. (4)) and crystal ion radii estimated from X-ray diffraction [59]

Anions	Hydrodynamic radius (nm)		Crystal ion radius (nm)
	H_2O	MeOH	
Br^-	0.118	0.262	0.196
I^-	0.120	0.242	0.220
NO_3^-	0.129	0.249	0.179
SCN^-	0.139	0.245	0.213

values are, however, relatively small and of the same order of magnitude for each anion and for both ethanolamine and ammediol counter-ions. Thus, for such K_{IP} values and in the conditions of this study, the association rates would be of 1.5–6% in ethanolamine-based BGE, and of 3–8% in ammediol-based BGE, according to the analyte. Eventually, in the range of ionic strengths and methanol/water compositions experienced in this study, the ion-pair phenomenon should influence the actual mobilities of the four inorganic anions to a very minor extent.

3.4. Evaluation of solvation effects

3.4.1. Evaluation of solvated radii from the Stokes model

As a starting point in the evaluation of solvation effects on electrophoretic mobilities, the solvated radii of the model anions were first assimilated to Stokes hydrodynamic radii, as defined by Eq. (5). This model stands for spherical particles having a size smaller than the Debye length, for which the electrophoretic friction coefficient is assimilated to the hydrodynamic friction coefficient. For each inorganic anion, the hydrodynamic radii were thus calculated from the absolute mobilities in water [59] and in methanol (this work) and the results were compared to the crystal ionic radii determined by X-ray diffraction (Table 4) [59]. It appears that the hydrodynamic radii in water are inferior to those in methanol, which could be explained by a greater solvation number in methanol, or by the volume difference between methanol and water molecules. It is also worth noting that the calculated solvated radii in water are lower than the crystal radii, which seems unrealistic. The Stokes model is, therefore, not applicable to these inorganic anions. Some of them, indeed, are not spherical in shape (SCN^- is ellipsoidal), and more generally it is known that the Stokes model underestimates the hydrodynamic radii of particles lower than 0.5 nm [58].

3.4.2. Evaluation of solvated radii from quantum models

To better understand the mechanisms ruling the electrophoretic migration of small inorganic anions, solvation was next studied at a microscopic level using a quantum first principle based on the DFT. Solvation was described as the formation of static ion–solvent clusters, which were considered to be stable when the energy for adding an extra solvent molecule is lower than the energy required to form a solvent dimer. The stabilizing energy ΔE_{stab} of a given cluster is thus computed as:

$$\Delta E_{stab} = E[\text{ion} - (S)_n] - E[\text{ion} - (S)_{n-1}] - E[S] \quad (6)$$

where $E[\text{ion} - (S)_n]$ and $E[\text{ion} - (S)_{n-1}]$ denote the energy of the clusters consisting of n and $n-1$ solvent molecules, respectively, and $E[S]$ is the energy of a solvent molecule. This microsolvation model works reasonably well for strongly interacting molecules [60], such as those belonging to the first solvation shell. It gives access to the solvation number, from which can be derived the cluster volume and the solvated radius, assuming a spherical shape. It must also be emphasized that a given cluster could have several conformations, all determined by local energy minima, the number of the accessible conformations increasing with the number of solvent molecules. Although different, the energies of these conformers were close to each other and it was verified in this work that their volumes varied by <1%. As we were mainly interested in this last parameter, the reference to these conformers was not mentioned in the following.

3.4.2.1. Solvated radii in water. The results for the stabilization energies of the anion–water clusters are reported in Table 5 together with the radii of the equivalent sphere. The most striking feature is the variable number of water molecules present in the first solvation shell, which ranges between two (bromide) and nine (nitrate). This behaviour is in agreement with the anion size and its polarizability (or better its hardness). So, bromide binds less water molecules (two versus four) than iodide, which is a softer anion, and the same is observed for the pair thiocyanate/nitrate (six versus nine). All these systems have a stabilization energy greater than the water–water interaction (-6.1 kcal mol^{-1},

Table 5
Characteristic parameters of the considered anion–water clusters for the first solvation shell (DFT calculations) and the bulk solvent effect (CPCM calculations): number of solvent molecules (n), stabilization energy (ΔE_{stab}) and solvated radius (r)

Anions	First solvation shell			Bulk solvent effect			Absolute mobilities in water (10^{-5} cm^2 V^{-1} s^{-1})
	n	ΔE_{stab} (kcal mol^{-1})	r (nm)	n	ΔE_{stab} (kcal mol^{-1})	r (nm)	
Br^-	2	−8.2	0.35	4	−9.7	0.38	80.9
I^-	4	−7.3	0.38	4	−8.2	0.40	79.2
NO_3^-	9	−6.6	0.47	8	−6.6	0.44	74.1
SCN^-	6	−9.2	0.42	8	−8.5	0.48	68.4

For comparison purposes, absolute mobilities in water at 25 °C [59] are also reported.

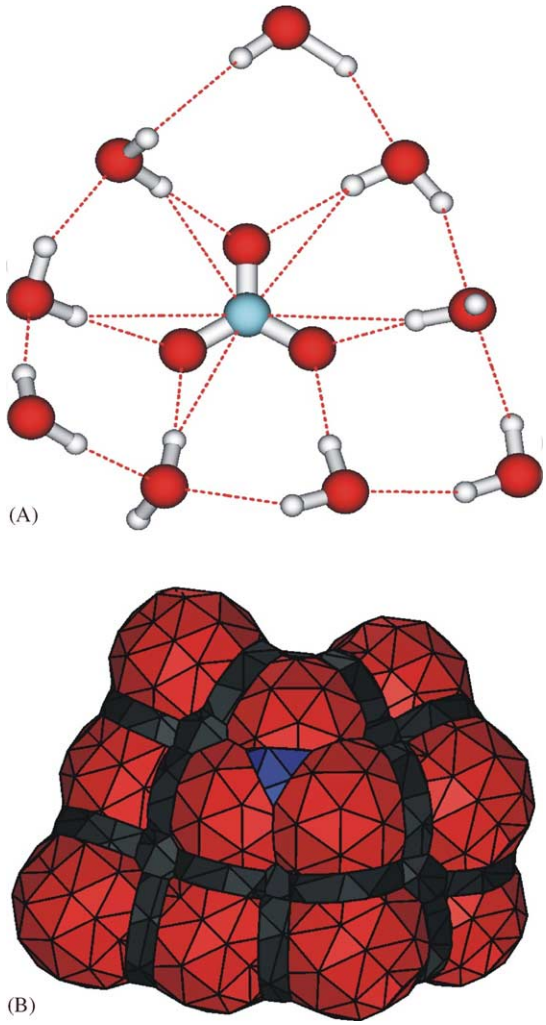

Fig. 5. Structure of: (A) the $[NO_3(H_2O)_9]^-$ complex according to the DFT model (short-range anion–solvent interactions solely) and (B) the $[NO_3(H_2O)_8]^-$ complex according to the CPCM model (long-range anion–solvent interactions included).

at the same calculation level; 1 cal = 4.184 J). The structure of the largest water cluster, $[NO_3(H_2O)_9]^-$, is depicted in Fig. 5A. The calculations also predict that the radii for the supermolecular complexes increase in the order $Br^- < I^- < SCN^- < NO_3^-$, while the order of decreasing absolute mobilities in water is $Br^- > I^- > NO_3^- > SCN^-$. An inverted order was, therefore, predicted for the pair thiocyanate/nitrate. This discrepancy suggests that more than one solvation shell may play a role and should be taken into account. Unfortunately, by the DFT model, it is quite tedious to process more explicit water molecules, because of the increasing number of local minima and the increasing computing time, both factors impeding a meaningful modelling of the chemical system. In order to introduce long-range molecular interactions in a cheap, yet effective, way we have used a continuum solvent model [42]. The results obtained for the optimized clusters (solute + explicit water molecules + continuum) are reported in the last three columns of Table 5. Significant variations in solvation number and radii are noticed using the CPCM approach: solvation numbers of Br^- and SCN^- increase with a concomitant increase in solvated radii. In the case of I^-, the solvation number remains unchanged, but the slight increase in solvated radii can be understood in so far as the solvating water molecules interact partly with the surrounding bulk molecules and less with the solute. These effects can be rationalized in terms of the effects of the solvent on the H-bond strengths. A polar solvent, like water, stabilizing electronic structures with charge separation (i.e. A^+X^- is more stable than AX in the presence of solvent) significantly increases the electrostatic contribution to the anion–water interaction energies [43]. This in turn induces shorter intermolecular distances between the anions and the water molecules, thus strengthening the small charge transfer component of the H-bond. The apparent discrepancy observed for the nitrate anion (from nine to eight molecules) is related to the higher steric hindrance of the crowed solvation shell, which increases in the presence of bulk effect due to, as for the other anions, the more compact rearrangement. The final result is a decrease of the number of waters with a concurrent decrease of the spherical radius (Fig. 5B). Most importantly for the purpose of this work, it appears now that the calculated radii (Table 5, last column) well agree with the expected reversed proportionality to absolute mobilities, as their product remained constant to within 3.8%, as illustrated in Fig. 6.

3.4.2.2. Solvated radii in methanol. The same theoretical approach was applied to the anion–methanol clusters. Considering the first solvation shell, the results obtained by DFT calculations for the solvation numbers, the stabilization energies and the solvated radii are given in Table 6. All the reported energies are slightly higher than the one characterizing a methanol–methanol interaction (-6.3 kcal mol^{-1} at the same calculation level). Except for NO_3^- it can be noted that the solvated radii are greater in methanol than in water, in accordance with the corresponding decrease in absolute mobility on going from water to methanol. For bromide, this increase in solvated radius is obviously due to the increase in solvation number. For the other three anions, the same variation should be due to the fact that the larger size

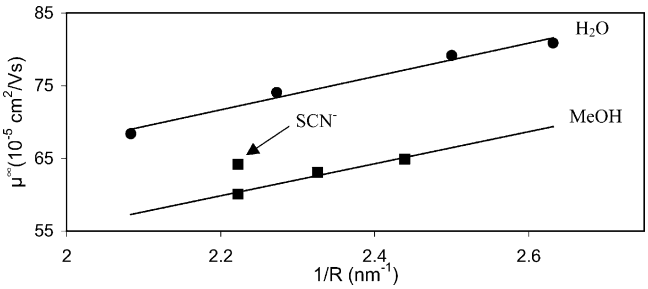

Fig. 6. Experimental absolute mobilities as a function of the reciprocal computed radii. The values in water were calculated with DFT coupled to CPCM models. The values in methanol were calculated from the DFT model.

Table 6
Characteristic parameters of the considered anion-methanol clusters for the first solvation shell (DFT calculations): number of solvent molecules (n), stabilization energy (ΔE_{stab}) and solvated radius (r)

Anions	First solvation shell			Absolute mobilities in methanol (10^{-5} cm^2 V^{-1} s^{-1})
	n	ΔE_{stab} (kcal mol^{-1})	r (nm)	
I^-	3	−7.9	0.41	64.9
SCN^-	4	−7.2	0.45	64.2
NO_3^-	3	−9.7	0.43	63.1
Br^-	3	−9.2	0.45	60.1

For comparison purposes, absolute mobilities in methanol at 25 °C [59] are also reported.

of methanol, as compared to water, overcompensates for the decrease in solvation number. Moreover, the solvated radii increase in the order $I^- < NO_3^- < Br^-$, SCN^-, while the order of decreasing absolute mobilities in methanol is $I^- > SCN^- > NO_3^- > Br^-$. Fig. 6 shows that the experimental absolute mobilities appear to be inversely proportional to the computed radius. Except for SCN^-, the product of the absolute mobility by the computed radius remained constant to within 1.2% which emphasizes the interest of this approach.

In order to take into account the solvent effect in methanol as we did in water, anion–methanol clusters were re-investigated using the CPCM model. Surprisingly at first glance, no cluster was found to be stable in a bulk methanol solution, since the computed stabilization energies turned out to be lower than that for the methanol–methanol interaction. In fact, the methanol molecules bound through hydrogen of the alcoholic group, the non-polar methyl pointing outside, toward the solvent. Consequently, intershell interactions are not ruled by the electrostatic contribution of hydrogen bonds any longer, but rather, by dispersion–repulsion forces. Unfortunately, these forces are hardly reproduced in the framework of a continuum model [42].

4. Concluding remarks

The selectivity alterations observed for the model inorganic anions (chloride, bromide, nitrate, thiocyanate) on varying the solvent composition (water–methanol mixtures) of the background electrolyte were interpreted in terms of ion-pairing and solvation phenomena. On one hand, the study of the variation of the electrophoretic mobilities of these four anions as a function of the concentration of the free counter-ion present in the electrolyte led us to infer that the actual mobility alterations due to ion-pairing between analytes and counter-ions remained minor, but their impact on migration orders can be significant, considering the low differences between them. On the other hand, the solvation effect on selectivity modification was shown to be even more important, through the predictions of theoretical microscopic quantum models yielding values for the solvated radius of each anion both in water and methanol. Except for one analyte, these models (density functional theory and conductor-like polarizable continuum model) turned out to be valuable tools for predicting the reverse proportionality of the absolute mobility to solvated radius, and it can be expected that they will soon become even more powerful regarding the complex ions in various pure or mixed solvents.

References

[1] I. Bjornsdottir, J. Tjornelund, S.H. Hansen, Electrophoresis 19 (1998) 2179.
[2] J. Senior, D. Rolland, D. Tolson, S. Chantzis, V.J. De Biasi, Biopharm. Biomed. Anal. 22 (2000) 413.
[3] S.P. Porras, I.E. Valko, P. Jyske, M.L. Riekkola, J. Biochem. Biophys. Methods 38 (1999) 89.
[4] S. Cherkaoui, J.L. Veuthey, J. Chromatogr. A 874 (2000) 121.
[5] T. Sokoliess, M. Gronau, U. Menyes, U. Roth, T. Jira, Electrophoresis 24 (2003) 1648.
[6] V. Piette, M. Lämmerhofer, W. Lindner, J. Crommen, J. Chromatogr. A 987 (2003) 421.
[7] Y. Hedeland, M. Hedeland, U. Bondesson, C. Pettersson, J. Chromatogr. A 984 (2003) 261.
[8] F. Wang, M.G. Khaledi, J. Chromatogr. A 875 (2000) 277.
[9] M. Grob, F. Steiner, Electrophoresis 23 (2002) 1921.
[10] D.L. Gallaher, M.E. Johnson, Anal. Chem. 72 (2000) 2080.
[11] T. Wang, H.S. Wei, S.F.Y. Li, Electrophoresis 19 (1998) 2187.
[12] Q. Yang, L.M. Benson, K.L. Johnson, S. Naylor, J. Biochem. Biophys. Methods 38 (1999) 103.
[13] K. Sarmini, E. Kenndler, J. Chromatogr. A 792 (1997) 3.
[14] H. Cottet, M.P. Struijik, J.L.J. Van Dongen, H.A. Claessens, C.A. Cramers, J. Chromatogr. A 915 (2001) 241.
[15] M.T. Bowser, E.D. Sternberg, D.D.Y. Chen, Anal. Biochem. 241 (1996) 143.
[16] T. Okada, J. Chromatogr. A 695 (1995) 309.
[17] T. Okada, J. Chromatogr. A 771 (1997) 275.
[18] H. Salimi-Moosavi, R.M. Cassidy, Anal. Chem. 67 (1995) 1067.
[19] N. Suzuki, Y. Ishihama, T. Kajima, N. Asakawa, J. Chromatogr. A 829 (1998) 411.
[20] K. Sarmini, E. Kenndler, J. Biochem. Biophys. Methods 38 (1999) 123.
[21] J.L. Miller, D. Shae, M.G. Khaledi, J. Chromatogr. A 888 (2000) 251.
[22] D. Barron, A. Irles, J. Barbosa, J. Chromatogr. A 871 (2000) 367.
[23] D. Barron, E. Jimenez-Lozano, A. Irles, J. Barbosa, J. Chromatogr. A 871 (2000) 381.
[24] P.B. Wright, J.G. Dorsey, J. High Resolut. Chromatogr. 21 (1998) 498.
[25] I. Bjornsdottir, S.H. Hansen, S. Terabe, J. Chromatogr. A 745 (1996) 37.
[26] S.P. Porras, M.L. Riekkola, E. Kenndler, Electrophoresis 23 (2002) 367.
[27] S. Descroix, A. Varenne, L. Geiser, S. Cherkaoui, J.L. Veuthey, P. Gareil, Electrophoresis 24 (2003) 1577.
[28] J.L. Miller, M.G. Khaledi, D. Shae, J. Microcol. Sep. 10 (1998) 681.
[29] J.L. Miller, M.G. Khaledi, D. Shae, Anal. Chem. 69 (1997) 1223.
[30] K.I. Roy, C.A. Lucy, Anal. Chem. 73 (2001) 3854.
[31] K.I. Roy, C.A. Lucy, Electrophoresis 23 (2002) 383.
[32] I. Bjornsdottir, S.H. Hansen, J. Chromatogr. A 711 (1995) 313.
[33] J. Muzikar, T. van de Goor, B. Gas, E. Kenndler, Electrophoresis 23 (2002) 375.
[34] M.T. Bowser, E.D. Sternberg, D.D.Y. Chen, Electrophoresis 18 (1997) 82.
[35] P. Debye, E. Huckel, Phys. Z. 24 (1923) 311.
[36] L. Onsager, Phys. Z. 27 (1926) 388.

[37] J. Bockris, K.N. Amulya, Modern Electrochemistry Ionics, Part 1, Plenum Press, New York/London, 1998.
[38] H. Falkenhagen, M. Leist, G. Kelbg, Ann. Phys. 11 (1952) 51.
[39] E. Pitts, Proc. Roy. Soc. (London) 217A (1953) 43.
[40] M. Stefansson, M. Novotny, Anal. Chem. 66 (1994) 3466.
[41] A. Warshel, Computer Modeling of Chemical Reactions in Enzymes and Solutions, Wiley, New York, 1991.
[42] J. Tomasi, M. Persico, Chem. Rev. 94 (1994) 2027.
[43] C. Adamo, A. di Matteo, P. Rey, V. Barone, J. Phys. Chem. A 103 (1999) 3481.
[44] S. Chalmet, M.F. Ruiz-Lopez, J. Chem. Phys. 115 (2001) 5220.
[45] I. Ciofini, C. Adamo, J. Phys. Chem. A 105 (2001) 1086.
[46] B. Mennucci, J. Am. Chem. Soc. 124 (2002) 1506.
[47] M.J. Frisch, G.W. Trucks, H.B. Schlegel, G.E. Scuseria, R.E. Stratmann, J.C. Burant, S. Dapprich, J.M. Millam, A.D. Daniels, K.N. Kudin, M.C. Strain, O. Farkas, J. Tomasi, V. Barone, M. Cossi, R. Cammi, B. Mennucci, C. Pomelli, C. Adamo, S. Clifford, J. Ochterschi, Q. Cui, P.M.W. Gill, B.G. Johnson, M.A. Robb, J.R. Cheeseman, T. Keith, M.K. Petersson, D.K. Malick, A.D. Rabuck, J.A. Montgomery, K. Raghavachari, M.A. Al-Laham, V.G. Zakrewski, J.V. Ortiz, J.B. Foresman, J. Cioslowski, B.B. Stefanov, A. Nanayakkara, J. Liu, A. Liashenklo, P. Piskorz, I. Komaromi, M. Challacombe, C.Y. Peng, P.Y. Ayala, W. Chen, M.W. Wong, J.L. Andres, E.S. Replogle, R. Gomperts, R.L. Martin, D.J. Fox, J.S. Binkley, D.J. DeFrees, J. Baker, J.P. Stewart, M. Head-Gordon, C. Gonzalez, J.A. Pople, Gaussian'98 (Revision A.7), Gaussian, Pittsburgh, PA, 1998.
[48] C. Adamo, V. Barone, Chem. Phys. Lett. 274 (1997) 242.
[49] A. Becke, Phys. Rev. A 38 (1988) 3098.
[50] C. Lee, W. Yang, R.G. Parr, Phys. Rev. B 37 (1988) 785.
[51] A. Frisch, M.J. Frisch, Gaussian'98 User's Reference, Gaussian, Pittsburgh, PA, 1998; and references cited therein.
[52] S.F. Boys, F. Bernardi F, Mol. Phys. 19 (1970) 553.
[53] V. Barone, M. Cossi, J. Tomasi, J. Comput. Chem. 19 (1998) 407.
[54] V. Barone, M. Cossi, J. Phys. Chem. A 102 (1998) 1995.
[55] C. Schwer, E. Kenndler, Anal. Chem. 63 (1991) 1801.
[56] W. Buchberger, P.R. Haddad, J. Chromatogr. 608 (1992) 59.
[57] Y. Yang, F. Liu, J. Kang, Q. Ou, J. Chromatogr. A 834 (1999) 393.
[58] R.A. Robinson, R.H. Stokes, Electrolyte Solutions, Butterworths, London, 1955.
[59] Y. Marcus, Ion Properties, Marcel Dekker, New York, 1997.
[60] D. Sicinska, P. Paneth, D.G. Truhlar, J. Phys. Chem. B 106 (2002) 2708.